Colloidal multiscale porous adhesive (bio)inks facilitate scaffold integration (F) (SCI)

Azadeh Mostafavi, (iD) Mohamadmahdi Samandari, Mehran Karvar, et al.

COLLECTIONS

(F)   This paper was selected as Featured

View Online   Export Citation   CrossMark

Colloidal multiscale porous adhesive (bio)inks facilitate scaffold integration Ⓕ SCI

View Online   Export Citation   CrossMark

Azadeh Mostafavi,[1,2] Mohamadmahdi Samandari,[3] iD Mehran Karvar,[4] Mahsa Ghovvati,[2] Yori Endo,[4]
Indranil Sinha,[4,a)] Nasim Annabi,[2,a)] and Ali Tamayol[1,3,a)] iD

AFFILIATIONS

[1]Department of Mechanical and Materials Engineering, University of Nebraska-Lincoln, Lincoln, Nebraska 68588, USA
[2]Department of Chemical and Biomolecular Engineering, University of California—Los Angeles, Los Angeles, California 90095, USA
[3]Department of Biomedical Engineering, University of Connecticut, Farmington, Connecticut 06269, USA
[4]Division of Plastic Surgery, Brigham and Women's Hospital, Harvard Medical School, Boston, Massachusetts 02115, USA

[a)]Authors to whom correspondence should be addressed: atamayol@uchc.edu; nannabi@ucla.edu; and isinha@bwh.harvard.edu

ABSTRACT

Poor cellular spreading, proliferation, and infiltration, due to the dense biomaterial networks, have limited the success of most thick hydrogel-based scaffolds for tissue regeneration. Here, inspired by whipped cream production widely used in pastries, hydrogel-based foam bioinks are developed for bioprinting of scaffolds. Upon cross-linking, a multiscale and interconnected porous structure, with pores ranging from few to several hundreds of micrometers, is formed within the printed constructs. The effect of the process parameters on the pore size distribution and mechanical and rheological properties of the bioinks is determined. The developed foam bioinks can be easily printed using both conventional and custom-built handheld bioprinters. In addition, the foam inks are adhesive upon *in situ* cross-linking and are biocompatible. The subcutaneous implantation of scaffolds formed from the engineered foam bioinks showed their rapid integration and vascularization in comparison with their non-porous hydrogel counterparts. In addition, *in vivo* application of the foam bioink into the non-healing muscle defect of a murine model of volumetric muscle loss resulted in a significant functional recovery and higher muscle forces at 8 weeks post injury compared with non-treated controls.

Published under an exclusive license by AIP Publishing. https://doi.org/10.1063/5.0062823

I. INTRODUCTION

Tissue engineering and regenerative medicine have demonstrated substantial promise for treating various diseases.[1] Engineering three-dimensional (3D), cell-laden scaffolds has been an important step in tissue engineering therapies.[2–4] The fabricated scaffolds should offer biological and physical properties that support cellular activities including migration, growth, differentiation, and maturation.[5,6]

Bioprinting technologies have received significant attention in tissue engineering due to their ability to fabricate complex constructs by precise deposition of bioinks to form 3D constructs.[7,8] Among various bioprinting approaches, extrusion-based bioprinting has attracted more attention due to its compatibility with a wide range of bioink viscosities, decent reliability, and capability of large-scale scaffold fabrication with clinically relevant dimensions.[9,10] Extrusion-based bioprinters also allow the fabrication of multi-materials scaffolds.[7,11] However, the quality of printing and the system reproducibility heavily depend on the bioink characteristics.[12]

Various biomaterials have been implemented for the 3D bioprinting of tissue engineering scaffolds. Among them, hydrogels have been broadly applied as bioinks due to their similarity to the native extracellular matrix (ECM) and tunability of their properties.[13,14] Hydrogels are networks of hydrophilic polymer chains with nano- to micro-scale porous structures.[15,16] Their porous structures allow gas and small molecules to diffuse throughout the network, providing a nurturing environment for the encapsulated cells.[17,18] However, by increasing the bulk size of the hydrogel scaffold, the diffusion capability is severely diminished, resulting in cell death within the depth of the construct.[19] In addition, poor cell infiltration and spreading within these hydrogels further limit early vascularization and innervation, thus impairing the viability and functionality of encapsulated cells.[20,21] Incorporation of micro to millimeter-scale channels within the hydrogel, through multi-material extrusion 3D bioprinting, is a possible resolution.[7] However, the engineered porosity using these techniques can negatively influence the mechanical properties, fidelity, and structural

stability of the final scaffold. Therefore, a high concentration of the hydrogel bioinks is required to stabilize the printed structures, which in turn limits cell spreading, migration, and tissue integration.[22–25] While pre-vascularization and pre-innervation strategies can also be implemented,[26] these strategies make the 3D bioprinting and subsequent tissue implantation highly complex.

An alternative approach to overcome these challenges is introducing interconnected multiscale pores within the hydrogel network to allow efficient mass transport and rapid cell infiltration. The presence of these pores would also offer more cell anchoring surfaces and therefore facilitate cell expansion, proliferation, and tissue regeneration.[20] In contrast to regular hydrogels, it has been shown that macroporous hydrogels enhanced cellular ingrowth.[27] Several techniques have been developed to generate macroporous hydrogels, such as freeze-drying,[28] gas foaming,[29] and agent leaching strategies.[30,31] However, most of these approaches are not compatible with 3D bioprinting as they involve the use of toxic materials that can negatively impact the encapsulated biological materials.[32] Alternatively, microgel-laden bioinks and aqueous-biphasic systems are reported, which allow cell incorporation during macroporous bioink preparation; however, these approaches demand multiple washing steps of the hydrogel structures to remove the sacrificial polymer, making them unsuitable for *in vivo* printing applications.[13,33,34] Recently, an approach has been developed based on the introduction of air bubbles into the hydrogel through a pulling/pushing procedure of the solution using a syringe. Although the formed bubbles enhance cell viability in the core of the hydrogel, there was no control over the bubble (pore) sizes and distribution.[35]

In this study, inspired by whipped cream production, we developed porous bioinks through a single step foaming process without using any toxic material. To form porous bioinks, the prepolymer solution was mechanically agitated by simple stirring, at relatively high rates, to generate a foam with a uniform, interconnected pore structure and porosity up to 80%. The foam bioink, which acted as a shear-thinning material, was used for 3D bioprinting of cell-laden constructs [Fig. 1(a)]. Gelatin methacryloyl (GelMA) was used as the hydrogel solution for the adhesive foam preparation due to its promise in various tissue engineering applications.[15,36] In addition, in our previous studies, we demonstrated the application of GelMA as tissue adhesives and sealants.[37–39] However, the pore sizes of GelMA adhesives, like other hydrogels, are smaller than cells, which may limit cellular growth and spreading inside the hydrogel network. The physical and mechanical properties of the adhesive foam generated from three different concentrations of GelMA prepolymers were characterized and compared to the GelMA hydrogel. The printability of the foam bioinks was then investigated with a 3D bioprinter as well as a custom-built handheld bioprinter.[40] The biocompatibility of the developed foam bioink was further assessed *in vitro* and *in vivo* through subcutaneous implantation in a rat model. The engineered foam bioinks have potential to be used for 3D printing of various cell-laden tissue constructs due to their tunable porosity, printability, biocompatibility, and the high potential of remodeling and regeneration by allowing cell infiltration into the printed structures. To determine whether the foam scaffold could confer functional tissue regeneration, we evaluated the ability of *in vivo* printed foam scaffolds to promote skeletal muscle regeneration in a murine model of volumetric muscle loss (VML).

II. RESULTS

A. Bioink preparation and physical characterization

Whipped cream is a colloid made of air bubbles wrapped with protein and lipid shells in an aqueous environment, which is usually formed by the vigorous stirring of cream. Whipped cream is easy-to-shape, easy-to-extrude, and maintains its structure after extrusion. Once stabilized, it forms a porous 3D structure. Inspired by this process and interesting characteristics of whipped cream, GelMA prepolymer solution was agitated using a homogenizer at high speed to form a foam. To increase the stability of the foam, 1% (w/v) polyvinyl alcohol (PVA), a synthetic biocompatible polymer, was added to the solution as a surfactant.[41,42] PVA has been widely used as a surfactant or foaming agent due to its water solubility, biocompatibility, and amphiphilic properties. Fourier-transform infrared spectroscopy (FTIR) was performed to evaluate the interaction of GelMA and PVA (Fig. S1). While non-covalent interactions between PVA and GelMA are expected, the results did not show a major shift in spectra as would be expected from chemical bonds.

The GelMA foam was then used a bioink to form cell-laden constructs using two different bioprinters: a 3D stationary printer and a handheld bioprinter. Figure 1 demonstrates an overview of the preparation process of cell-laden foam bioinks for 3D bioprinting of multiscale porous constructs. After foaming, cells can be mixed with the foam bioink and printed using a 3D stationary or a handheld bioprinter [Fig. 1(a)]. The hierarchically distributed macro- to micropores within the 3D printed scaffolds are shown in Fig. 1(b). The representative bright-field micrograph in Figs. 1(b)–1(i) shows the macroporous ($\geq 500\,\mu m$) structure formed through the extrusion 3D bioprinting process. Representative scanning electron microscopy (SEM) images from 3D printed filaments [Figs. 1(b-ii) and 1(b-iii)] exhibited the interconnected mesoscale pores (50–400 μm) generated during the foaming process and the microporous structure [Fig. 1(b-iv)] of the cross-linked GelMA hydrogel.[16] The microporous structure further enables the interconnectivity of the mesoporous structure through small inherent GelMA pores.

The visual and quantitative representations of the pore size distribution inside the foam bioink are shown in Figs. 2(a) and 2(b), respectively. As expected, the pore size was decreased with the increasing stirring time [Figs. 2(a-i) and 2(b-i)], stirring speed [Figs. 2(a-ii) and 2(b-ii)], and the concentration of the hydrogel [Figs. 2(a-iii) and 2(b-iii)], while the effects of stirring speed and hydrogel concentration were more significant. This fact demonstrates the shear-dependent mechanism of microbubble formation in the foaming process. During this process, a large amount of air is first introduced into the liquid through stirring at the liquid-air interface. Subsequently, the captured bubbles inside the liquid are split into smaller bubbles because of shear stress dominating the surface tension of the bubbles.

Increasing the stirring speed and hydrogel precursor concentration directly increased the shear stress applied to the bubbles during the foaming process and therefore reduced the bubble size [Figs. 2(a-ii), 2(a-iii), 2(b-ii), and 2(b-iii)]. While most of the bubbles could quickly breakup by the shear stress caused by mechanical stirring, the longer duration of shear force exertion resulted in further splitting of bubbles. Therefore, the time of the stirring affected the dispersity of the size distribution, which was correlated with the width of normal distribution graphs shown in Fig. 2(b). Our results demonstrated that while increasing the stirring time could decrease the size
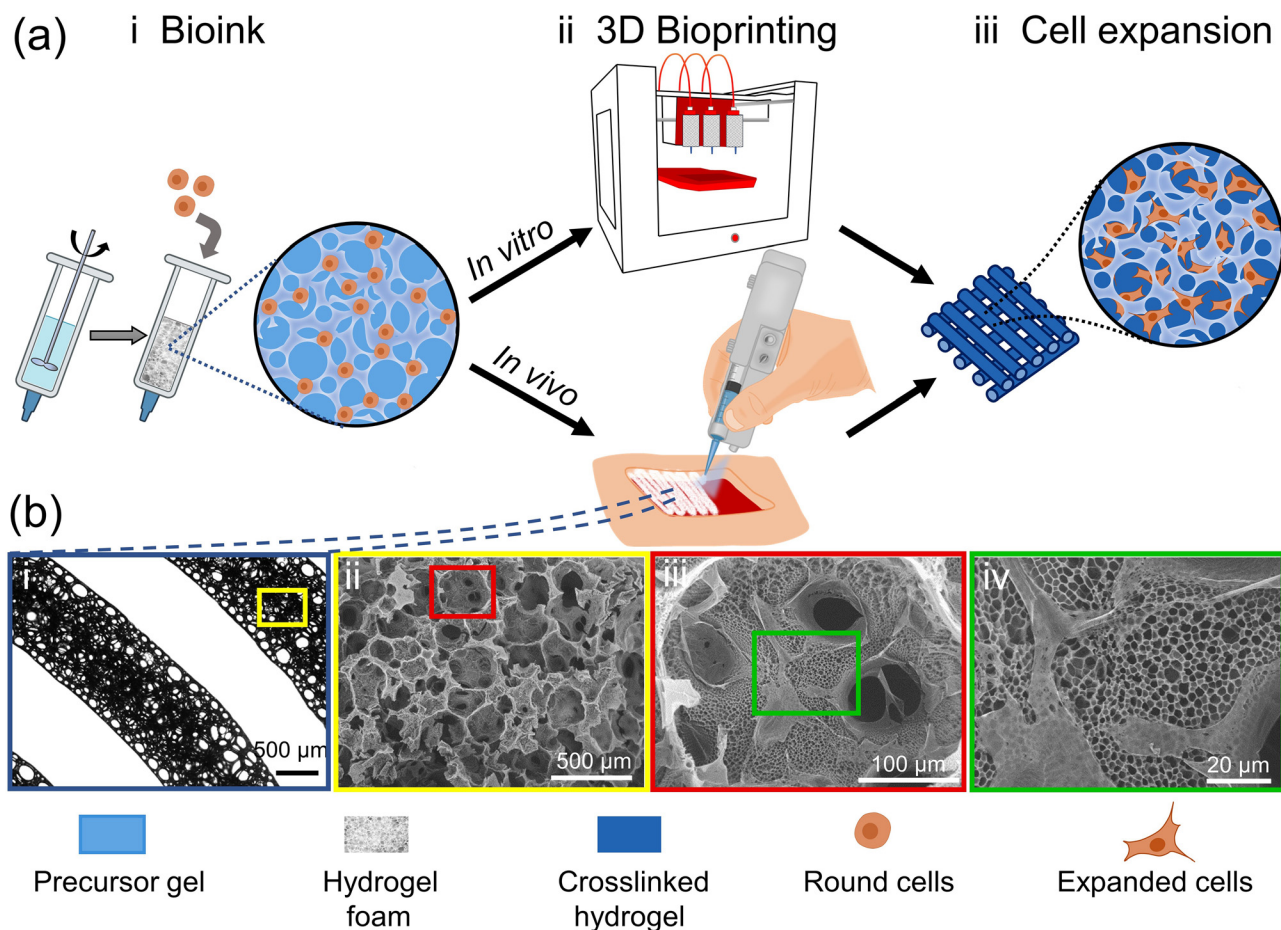
FIG. 1. The concept of engineering an adhesive foam bioink for 3D bioprinting inspired by whipped cream formation. (a) Schematic illustration of 3D bioprinting of multiscale porous structures using the adhesive foam-based bioink. (i) The preparation process of the cell-laden adhesive foam bioink through hydrogel precursor stirring followed by cell addition; (ii) 3D bioprinting of the foam bioink *in vitro* using a stationary bioprinter or *in vivo* utilizing a handheld bioprinter; (iii) Multiscale porous structure of the bioprinted foam, facilitating cell expansion in the printed constructs. (b) The micrographs from hierarchical macro- to micro-scale pores within the 3D printed scaffolds: (i) a representative bright-field microscopy image from macroporous 3D printed structure; (ii–iv) representative SEM images from printed foam bioink filaments, (ii and iii) interconnected mesoporous structure formed by foaming process, (iv) microporous GelMA structure formed after cross-linking of the polymer chains.

dispersity, even a 20 s stirring generated an almost homogeneous structure in a 15% GelMA foam when a 15 000 rpm was used [Figs. 2(a-i) and 2(b-i)]. The significant change in pore size distribution by varying the stirring speed and hydrogel concentration further showed that the required time for obtaining a homogeneous foam structure was shear dependent. Higher shear stress rates due to the faster stirring speed [Figs. 2(a-ii) and 2(b-ii)] and hydrogel concentration [Figs. 2(a-iii) and 2(b-iii)] could decrease the required time for the formation of foam with monodisperse pore size.

Furthermore, the pores preservation in the foam bioink during the extrusion process of printing and the scaffold stability in physiological conditions were assessed. Rhodamine B-loaded GelMA foam was printed, incubated in Dulbecco's phosphate-buffered saline (DPBS) solution at 37 °C for 1 h, and imaged with a fluorescent microscope [Fig. 2(c)]. The micrographs showed that the pores were stable in the printed filaments and the pore size distribution was homogenous. Furthermore, we observed that the porous scaffolds were stable

after incubation at 37 °C. A higher magnification micrograph shown in Figs. 2(c)–2(i) indicates the interconnectivity of the pores within the printed structure.

The formation of a mesoporous structure within biofabricated scaffolds is an important factor since it supports cellular ingrowth within the scaffold without the need for scaffold degradation. The density and porosity of the printed foam bioink were further evaluated and compared with the GelMA hydrogel. As expected, the density of foam bioink was significantly lower than their GelMA counterparts, which is associated with the integration of air bubbles into the bioink during the foaming process [Fig. 2(d)]. The calculated porosity of the foam bioinks was around 75%, 68%, and 65% for the foams generated from 10%, 15%, and 20% (w/v) GelMA, respectively [Fig. 2(e)]. This clearly demonstrates the significant increase in free space available for cellular ingrowth in the printed foam bioink.

The mass change of the scaffolds was also measured over time (Fig. S2). Two conditions were considered for this experiment: (i)
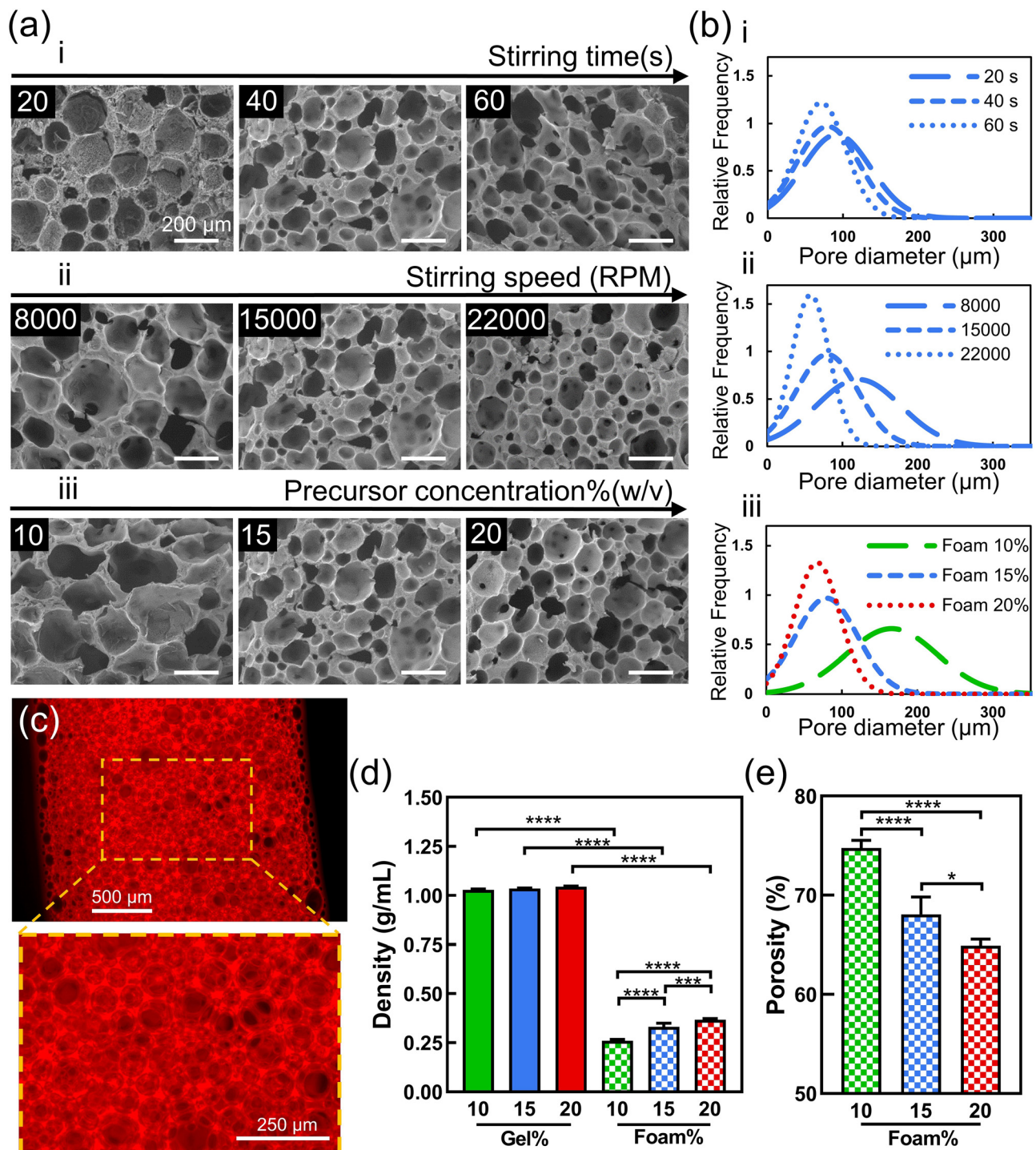
FIG. 2. Characterization of porosity in the printed foam constructs. (a) Tunability of the pore size and distribution within the foam bioink through manipulation of (i) stirring time, (ii) stirring speed (RPM), and (iii) hydrogel precursor concentration. (b) Quantitative representation of pore size distribution corresponding to groups showed in panel a (n = 3). (c) Representative fluorescent images from Rhodamine B-loaded foam filaments demonstrating the stability of the interconnected pores after extrusion and 1 h incubation in DPBS at 37 °C. (d) Comparison between the density of the hydrogel and foam bioinks (n = 4). (e) Calculated porosity in foam bioinks made with different GelMA concentrations (n = 4). (p < 0.05 is denoted by *, and p < 0.01 and p < 0.0001 are denoted by ****).

incubation in DPBS and (ii) incubation in DPBS containing collagenase type I to mimic expedited degradation of gelatin-based materials *in vivo*. Samples were incubated at 37 °C and weighed at each time point. The results demonstrated that foam scaffolds experienced a significant mass increase in DPBS solution over time compared to the Gel scaffolds [Fig. S2(a)]. This is mainly due to the hydration of the scaffold through replacement of the entrapped air with the solution in the environment as a result of the hydrophilicity and interconnectivity of the polymeric network. On the other hand, in the presence of collagenase [Fig. S2(b)], the degradation of the 10% (w/v) GelMA foam scaffold was much faster than its counterpart gel scaffold. The mass change ratio in the foam samples made of 15% (w/v) and 20% (w/v) GelMA initially increased slightly (31 ± 8% after 24 h in foam samples with 20% GelMA); this suggests that swelling dominated the degradation at earlier time points. However, samples' mass started to decrease after 24 h, and a comparable mass change between the foam samples and hydrogel scaffolds was observed in later time points. Both foam and hydrogel scaffolds containing 15% (w/v) GelMA and 20% (w/v) GelMA entirely degraded after 96 h and 120 h, respectively. The mass changes of the samples were also measured in DPBS without collagenase to assess their long-term stability. The results indicated that foam scaffolds made from 10% (w/v) GelMA degraded after 8 days, suggesting limited stability (Fig. S3). Additionally, the mass of the foam samples made from 15% (w/v) and 20% (w/v) GelMA increased up to 9 days and then started to decrease (Fig. S3). Overall, both 15% (w/v) and 20% (w/v) GelMA foam samples were stable for at least 42 days. These results suggested that the foam structures made of 10% (w/v) GelMA solution were not stable enough for most tissue engineering applications.

To evaluate the swelling behavior of the printed foam scaffolds, samples were incubated in DPBS for 48 h. The results indicated a higher swelling ratio in foam scaffolds with lower hydrogel concentrations. The swelling ratio increased to 499 ± 20% after 48 h in foam samples made of 10% (w/v) GelMA, which was only ∼1% in hydrogel scaffolds with the same concentration [Fig. S2(a)]. The swelling ratio in foam scaffolds made of 15% and 20% (w/v) GelMA were 121 ± 26% and 66 ± 31%, respectively.

B. Characterization of the mechanical properties of the foam scaffolds

Although increased porosity of the printed scaffolds can improve the cell permissibility and mass transport through the structure, it might have negative effects on the mechanical stability of the printed constructs. Therefore, the mechanical properties of the scaffolds fabricated from foam bioinks with different GelMA concentrations were assessed and compared with bulk hydrogel samples [Figs. S2(c) and S2(d)]. The results of the compression test indicated that Young's modulus in the printed foam scaffold increased from 4 ± 4 to 46 ± 33 kPa, and 102 ± 26 kPa by changing the GelMA concentration from 10% to 15%, and 20% (w/v), respectively [Fig. S2(c)]. Overall, foam scaffolds showed lower Young's modulus in comparison with hydrogel samples. The compressive moduli of the foam scaffold was in the range of values or soft tissues.[43] While a minimum mechanical stiffness is required for fidelity and stability of the printed constructs, usually high mechanical properties are not favorable for 3D cell-laden scaffolds applied in soft tissue regeneration due to their limited cell permissibility, as well as lack of similarity between the scaffold and native tissue, which can significantly affect cellular behavior. We further evaluated the effect of pore size on the mechanical properties of the resulting foam hydrogels by changing the stirring speed for foaming [Fig. S2(e)]. The results showed that while the mechanical properties could change with the pore size, the difference was not statistically significant.

Furthermore, cyclic compression tests were performed to evaluate the mechanical hystersis of the scaffolds and their ability to withstand repetitive loading and unloading forces applied to the implanted scaffolds during body motion. Cyclic compression tests were performed at 50% strain up to 20 cycles. Interestingly, the foam samples could sustain the cyclic loading without significant changes in their stress-strain curves, while 10% (w/v) hydrogel scaffolds broke at the first cycle. Figure S2(d) demonstrates the stress-strain plots obtained during the 10th loading cycle. Similar to the normal compression tests, decreasing in stiffness of the scaffold was observed with reducing the GelMA concentration. The results indicated that although 10% (w/v) GelMA foams had more ductility than 10% (w/v) hydrogel scaffolds, due to its lack of stability, it is not suitable for tissue engineering applications.

C. Characterization of the rheological properties and the printability of the foam bioinks

The rheological properties of the bioinks significantly affect their printability. While GelMA is a promising material for forming 3D cell-laden scaffolds, its low viscosity and slow photocross-linking limited its application as a bioink in bioprinting.[44] A strategy to resolve this problem is partial thermal cross-linking of the hydrogel precursor by decreasing the temperature.[44] However, the rapid sol–gel transition of GelMA at low temperature could cause complete thermal cross-linking and therefore increased the viscosity during printing. This could also limit the printability window and makes the GelMA bioprinting unreliable. Figure 3(a) shows the storage and loss moduli of the GelMA, in comparison with foam bioink with similar GelMA concentration. The results confirm that the decreasing temperature induces the transition of both GelMA and foam from solution phase to solid phase, as suggested by larger storage modulus in lower temperatures in comparison with loss modulus. The storage modulus of 15% GelMA bioink experienced around 1000-fold increase during its sol–gel transition between 30 and 25 °C, making the bioprinting of partially gelled bioink highly unstable. On the other hand, there was only 14-fold increase in the storage modulus of a 15% GelMA foam bioink during the sol–gel transition in the same temperature range, which made it much easier to print using our partial gelation strategy.

Increasing the GelMA viscosity by enhancing its concentration is another possible solution to facilitate its 3D printing; however, it causes poor cellular activity and spreading upon photocross-linking as a result of high mechanical properties.[25] Figure 3(b) compares the viscosity of the gel and foam bioinks with similar concentrations (15%). Interestingly, the viscosity of the foam precursor was on the order of 2 Pa·s, which was 30 times higher than the GelMA precursor (∼0.07 Pa·s), enabling the facile 3D bioprinting of the foam bioink. Furthermore, lower mechanical properties of the foam along with the presence of intrinsic pores, described previously, can improve the cellular activity within this bioink compared to the GelMA, reducing the challenge of cell permissibility in concentrated GelMA bioinks used for enhanced printability.
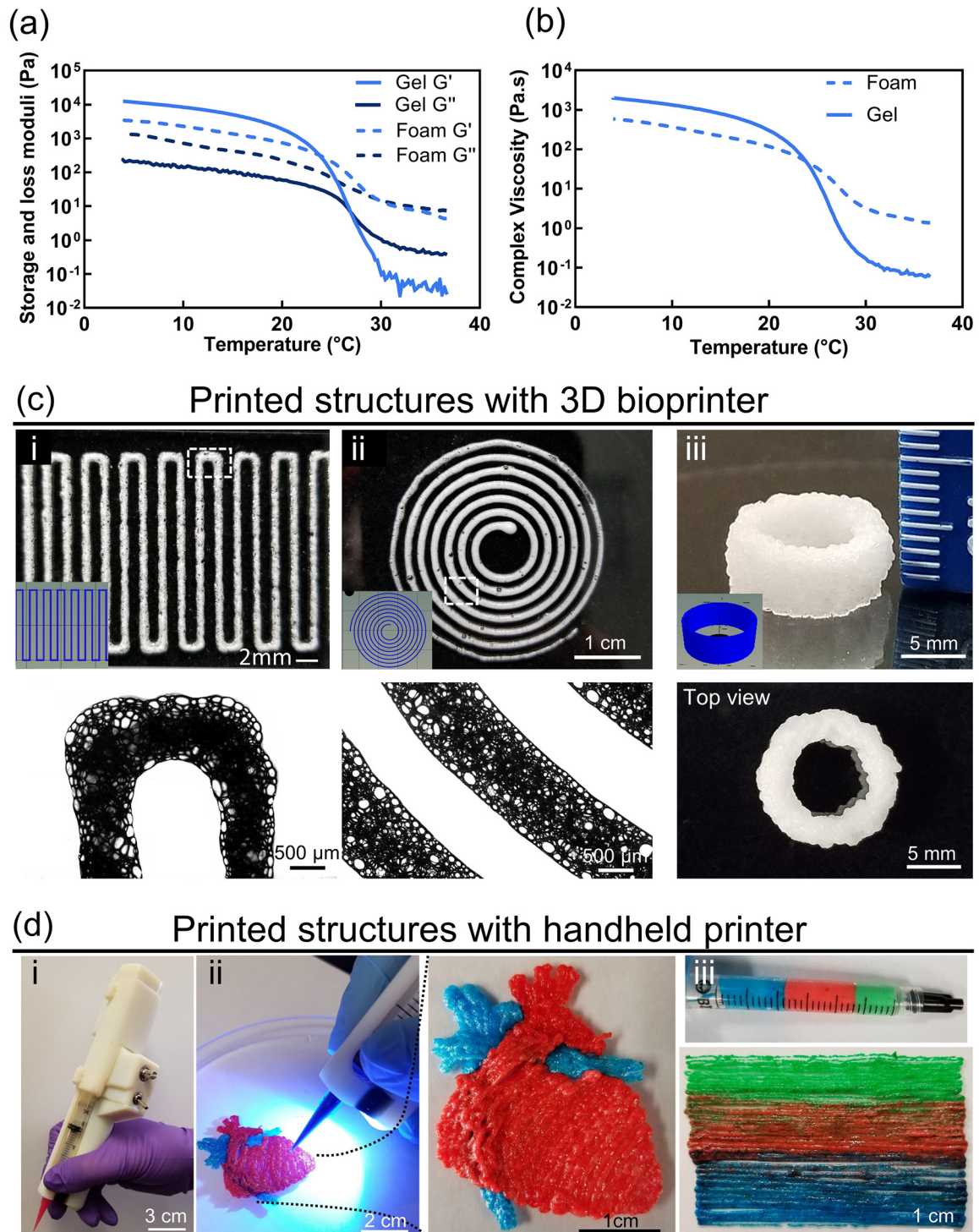
FIG. 3. 3D printing of the foam bioink using stationary and handheld bioprinters. Rheological parameters including (a) storage and loss moduli, and (b) bioink viscosity were compared between the foam and bulk bioinks. (c) Various printed 3D structures with foam bioink using a stationary 3D bioprinter: (i, ii) zigzag and spiral printed patterns and their corresponding designs; (iii) a multi-layered (16 layers) hollow cylinder printed construct as a free-standing 3D structure. (d) 3D printing of foam using a handheld printer. (i) The custom-built handheld printer; (ii) a 3D heart shape structure printed with two different foam bioinks, followed by their *in situ* cross-linking using an embedded UV cross-linking light; (iii) field syringe with three color of foam bioink which did not blend to each other and continued printed filaments structure from the same syringe to show that ability of gradient printing with foam bioinks.

The printability of the foam bioink was validated by assessing the quality of the printed 3D structures using a commercial extrusion-based 3D bioprinter [Figs. 3(c) and S4]. As shown by bright-field microscopic images of the 3D printed structures, the foam filaments had a consistent thickness and porosity distribution. This implies that the incubation period inside the 3D printer and extrusion process even from a relatively narrow tip (250 μm) had no effects on the foam and deposited filament structures. In order to assess the feasibility of using the foam ink for printing 3D structures, a multi-layer (consists of 16 layers) hollow cylinder, with 9 mm inner diameter, 1 mm thickness, and 5 mm height, was constructed. As shown in Fig. 3(c-iii), the foam bioink allowed the fabrication of a 3D structure with good fidelity without requiring any supporting material or structures. Increased viscosity of the foam along with rapid sol–gel thermal transition upon printing offered facile 3D printing of the constructs with high structural stability, even before photocross-linking. The rapid sol–gel transition was due to low density of the foam bioink, enhancing its surface-area-to-volume ratio, and consequently accelerating the temperature decrease. The printing parameters including temperature, pressure, and speed were optimized for enhanced printability of the foam bioink with continuous filament structure, preventing any "overflowing" or "dash-printed" patterns (Fig. S4). The best printing quality was obtained at 9 PSI extrusion pressure, 5 mm·s^{-1} printing speed, printing in ambient temperature (22 °C), and extrusion through a 25-gauge tapered plastic tip. Representative micrographs of three different printed architectures are demonstrated in Figs. 3(c-i) and 3(c-iii).

As direct *in vivo* printing of scaffolds has drawn significant attention recently, the suitability of the engineered foam bioink for *in vivo* printing applications was explored using a partially automated custom-built handheld printer[40,45,46] [Figs. 3(d)–3(i)]. The flow rate was set to 5 μL/s, and a 22G tapered plastic tip was used as the nozzle. Figure 3(d-ii) illustrates a heart shape structure printed with two different colored foam bioinks to show the quality of the printing using a handheld bioprinter.

For many tissue engineering applications, graded structures with gradient factors are required to enable the reconstruction of different tissue interfaces.[47] However, a multi-head bioprinter with the capability of multi-material bioprinting is not always accessible. If the printer does not offer such capability, the bioprinting of graded structures is extremely challenging as the inks carrying different cells or active molecules cannot be kept distinctly in a single container. However, in the case of our foam inks, the mixing of the different inks can be minimal and therefore, graded structures can be printed using any printers. To demonstrate this capability, three food colors were added to the foam bioinks which were loaded into a syringe one after another to print a continuous filament [Fig. 3(d-iii)]. The printed structure showed that the bioinks with different colors did not mix with each other under printing pressure or during the extruding process. It is noteworthy that only slight mixing of the colors happened in the transition part of the bioinks from one to another. This ability to avoid mixing of reagents creates a unique opportunity to print graded scaffolds. Creating such graded scaffolds is challenging by regular hydrogel bioinks. Such graded scaffolds could be used in many applications that the interface between multiple tissues should be restored.

D. Adhesion of the foam scaffold to the tissues

In situ printing can offer a rapid treatment with a high level of controllability and flexibility over the printing within irregular-shaped

defects. *In situ* printing of adhesive materials and further cross-linking of the structure can minimize the requirement of fixation modalities of the implanted structure. The application of adhesive materials for *in situ* printing enhance the implant-tissue integration since it prevents implant slippage during the body movement. Because most hydrogels are not suturable, their adhesion to the surrounding tissue is highly important for their application in regenerative medicine. GelMA hydrogel is known to adhere to the live tissues if cross-linked *in situ*.[40,48] To assess the adhesion of the foam ink upon *in situ* cross-linking, the adhesion strength of the bioinks to natural tissues (porcine skin) was measured using a lap shear test [Figs. 4(a) and 4(b)]. The results demonstrated that the foam samples broke from the bulk structure rather than the tissue-scaffold interfaces, indicating a cohesion failure mechanism [Fig. 4(a-ii)]. In addition, the adhesion strength of the foam bioinks increased from 4 ± 3 to 6 ± 1 kPa, and 14 ± 3 kPa, by increasing the concentration of GelMA from 10% to 15% and 20% (w/v), respectively [Fig. 4(b)]. On the other hand, the bulk hydrogel samples failed at the hydrogel–tissue interface, showing an adhesion failure mechanism [Fig. 4(a-iii)]. The results showed that the adhesion strength of GelMA bulk hydrogels was higher than the foam samples.

To further evaluate the adhesion of the foam and hydrogel scaffolds, shear strain and toughness were also calculated in the lap shear test [Figs. 4(c) and 4(d)]. The results revealed that although the shear strength of the foam was less than GelMA hydrogels, the total dissipated energy during the foam sample failure was higher than the bulk hydrogel [Fig. 4(c)]. A higher shear strain of the foam samples as compared to hydrogel further confirmed the previous results, demonstrating higher flexibility of foams compared to hydrogels [Fig. 4(d)]. This indicates that foam can be easily applied for the regeneration of soft tissues with significant deformation, such as the skin and muscle.

The feasibility of the *in vivo* printing process and adhesion of the printed structure to the surrounding tissue were evaluated in euthanized rats. VML and skin wound injuries were created on euthanized rats, and a handheld printer was used for *in situ* printing of the foam bioink directly within the defect site [Figs. 4(e) and 4(f)]. The printing procedure confirmed that *in vivo* printing of the foam bioinks using the handheld printers could form 3D scaffolds in a layer-by-layer fashion, which also adhered to the injury site and matched the irregular shape of the injured tissue.

E. *In vitro* biological characterization of the foam scaffolds

The physical and mechanical characterizations suggested that the constructs printed using 10% (w/v) foam bioink did not offer sufficient mechanical and adhesion strengths for most tissue engineering applications. On the other hand, while 20% (w/v) foams were stable and adhered well to the tissues, a lower polymeric concentration in bioinks is usually preferred for better cellular infiltration and spreading. Therefore, 15% (w/v) foam bioink was selected as the best concentration, and its biocompatibility was assessed both *in vitro* and *in vivo*. To evaluate the biocompatibility of the printed scaffolds formed by using the foam bioink, the viability and the metabolic activity of the cells were investigated using a Live/Dead® and a PrestoBlue® assays, respectively. C2C12 myoblasts and primary human mesenchymal stem cells were used for the *in vitro* biocompatibility assessment [Figs. 5(a) and S5]. Cells were encapsulated in 15% (w/v) foam and bulk hydrogel bioinks, printed on 3-(Trimethoxysilyl)propyl methacrylate
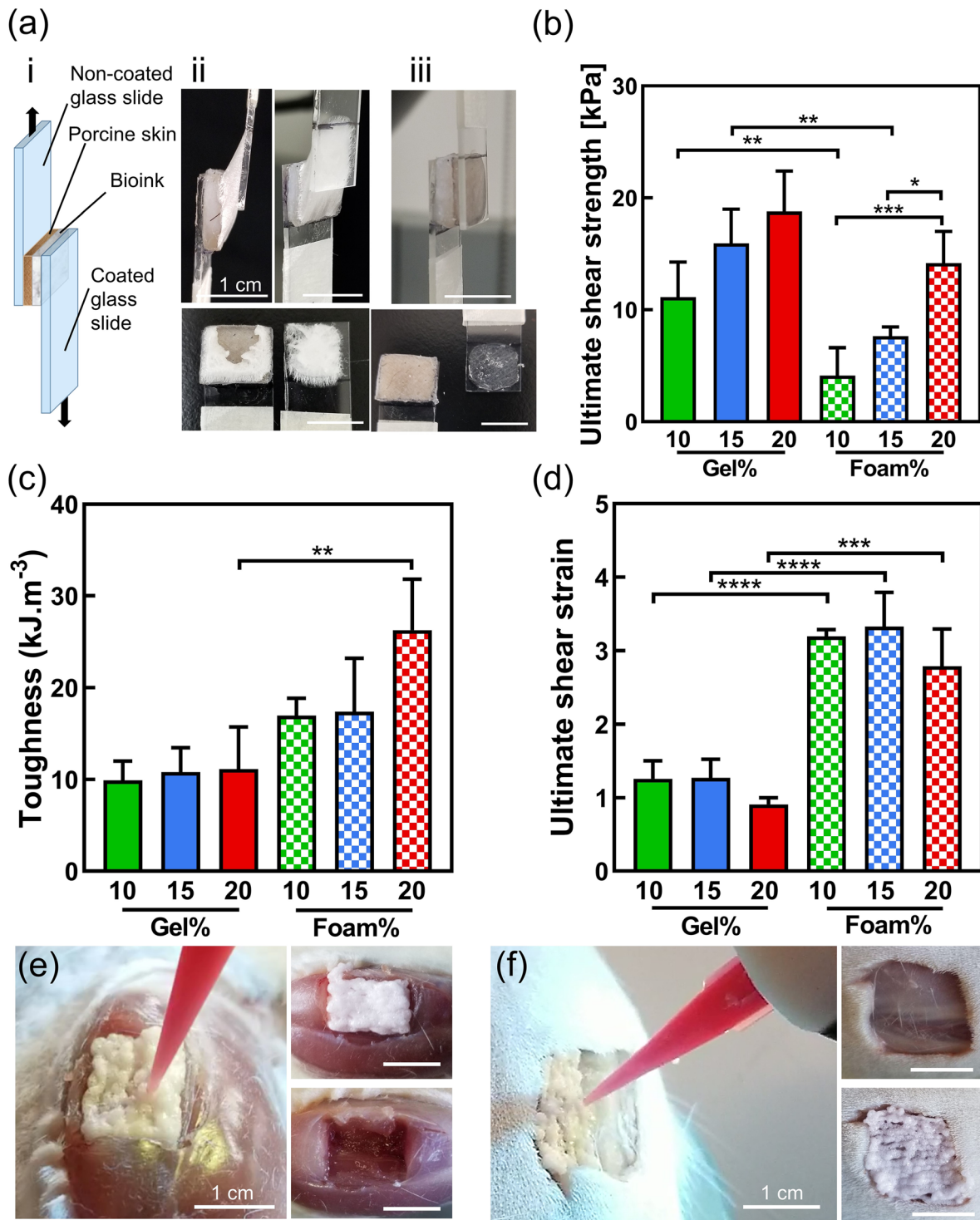
FIG. 4. Evaluation of the adhesion strength of the scaffolds formed with the foam bioinks. (a) Lap shear experimental setup, (i) a schematic representation of the lap shear test, (ii) the scaffold created by the foam bioink stretched under shear and ruptured from the bulk (cohesion failure), as compared to (iii) the hydrogel samples failed at the tissue-scaffold interface (adhesion failure). (b) The adhesion strength of the scaffolds to porcine skin. (c) Toughness and (d) ultimate shear strain of different foam and gel scaffolds, calculated from the lap shear test. (e) *Ex vivo* printing of the foam bioinks into induced VML and (f) wound injury to show the feasibility of foam *in vivo* printing and its adhesion to the surrounding tissue.
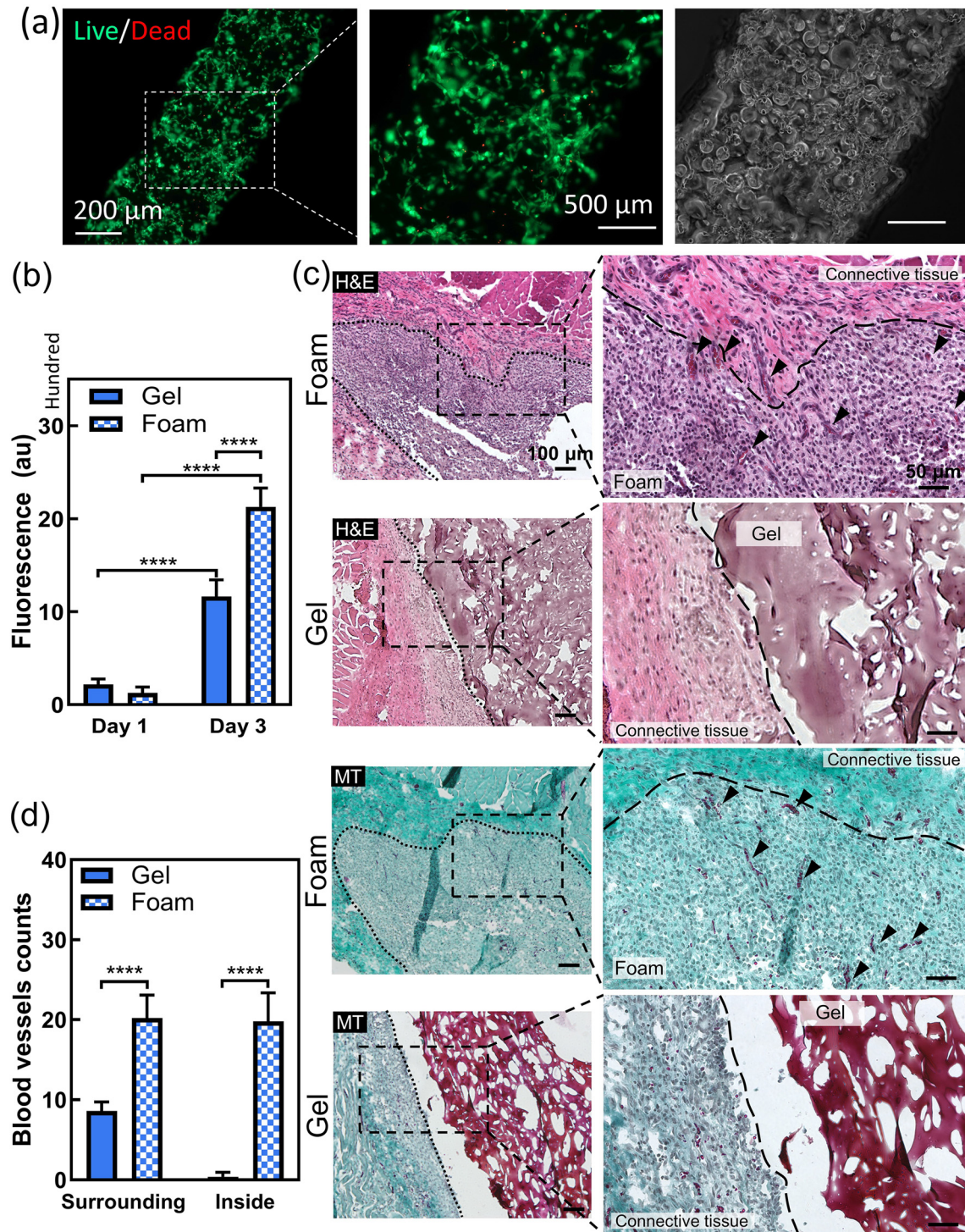
FIG. 5. *In vitro* and *in vivo* biocompatibility assessment of the foam scaffolds. (a) Live/Dead staining demonstrating the viability of the encapsulated cells (live: green, dead: red) in the foam scaffolds at day 1 post bioprinting. (b) The results of the PrestoBlue® assay, indicating cellular proliferation over 3 days in the foam and gel scaffolds. (c) Hematoxylin and eosin (H&E) and Masson's trichrome (MT) staining of the scaffolds-tissue interface 1 week post implantation. Black arrowheads pointing to neovessels formed in the foam scaffold, demonstrating the high level of foam-tissue integration. MT staining did not show a noticeable fibrotic capsule around foam and gel samples. (d) Quantitative evaluation of tissue vascularization in surrounding tissue and inside the implanted scaffold 1 week post implantation.

(TMSPMA)-treated slides, photocross-linked for 20 s, and incubated for up to 3 days. The micrographs from the stained samples with Live/Dead kit demonstrated that most of the cells were alive in both foam and bulk hydrogel scaffolds, demonstrating the biocompatibility of the materials and printing process [Figs. 5(a) and S5]. The staining further demonstrated cellular spreading inside the foam scaffolds, while cells remained round in bulk hydrogels, even after 3 days of culture. This indicates that the foam scaffolds provided a better environment for cells to spread in compared to bulk hydrogel. The proliferation and metabolic activity of the cells were also assessed by PrestoBlue® assay [Fig. 5(b)]. Overall, a superior proliferation was observed in the foam samples as compared to bulk hydrogel. This could be due to the porous structures of the foam scaffolds, which facilitated nutrients and oxygen transfer within the scaffolds and promoted cellular proliferation in 3D constructs. Moreover, a higher surface-area-to-volume ratio in foam structure could support cell expansion, without the need for scaffold remodeling, and enhance the cellular activity.

F. Subcutaneous implantation of foam scaffolds in rats

To investigate the biocompatibility and biodegradation and their ability to support *in vivo* regeneration, both foam and bulk hydrogels were implanted subcutaneously in rats and monitored for 4 weeks [Figs. 5(c) and S6(a)]. The foam constructs underwent a significant reduction in the bulk size as compared to gel samples. The representative micrographs from hematoxylin and eosin (H&E) as well as Masson's trichrome (MT) staining displayed mild inflammation in both foam and bulk hydrogel samples and their surrounding tissue including the presence of multinucleated giant cells, macrophages, fibroblasts, and collagen. The histology images showed that all the foam constructs were fully occupied by cells that infiltrated into the scaffolds after 1 week of implantation. Furthermore, a high number of microvessels within the foam scaffolds and their surrounding tissue were observed [Fig. 5(d)]. However, a few infiltrated cells were detected inside the bulk hydrogel samples. Additionally, the bulk hydrogels were intact and did not integrate with the host tissue. Four weeks post-implantation, foam samples were fully degraded, and newly regenerated tissue was replaced the scaffold. While the samples could not be found at day 28, H&E images from the tissue of the implanted area are provided in Fig. S6(b). On the other hand, the hydrogel samples were still present in subcutaneous tissue as a bulk scaffold at day 28 post-implantation. A slight degradation was observed in the bulk hydrogel and a small portion of the volume was infiltrated by cells. These results indicated that the multiscale interconnected pores in the foams could significantly increase cell infiltration, vascularization, and regeneration.

G. *In vivo* printing of adhesive GelMA foam scaffold in mice with VML injury

Using a validated murine model of VML, in which a reproducible composite defect is made within the posterior compartment of the lower hindlimb, we tested the efficacy of *in vivo* printing of the foam scaffold with regard to restoration of muscle function and structure.[49,50] Figures 6(a-i)–6(a-iii) demonstrate the process of simulate the VML injury using a biopsy punch to make a full thickness tissue defect in posterior compartment of the lower limb. The void area was filled with foam bioink filaments, parallel to nascent muscle, which

were printed using the handheld printer directly and cross-linked while the UV source were activated [Figs. 6(a-iv)–6(a-v)]. Animals were divided into three groups: (1) sham group with no muscle injury; (2) negative control, in which a 4 mm biopsy punch was used to create a full thickness VML injury in the posterior hindlimb compartment without applying any subsequent treatment; and (3) animals received a similar injury to group 2, but foam scaffolds were *in vivo* printed immediately following the injury. The animals were euthanized 8 weeks following the procedure to evaluate the level of muscle recovery. The gross pictures of harvested muscle tissues showed a significant defect in the non-treated group after 8 weeks. Interestingly, foam scaffold treatment of the injury site resulted in restoration of the normal muscle contour [Fig. 6(b-i)]. Qualitative histological assessment of muscle samples showed that the foam scaffolds were stable until 8 weeks and supported an excellent soft tissue regeneration at 8 weeks following VML injury [Figs. 6(b-ii)–6(b-iv)]. Specifically, MT staining demonstrated significantly less fibrosis in the animals treated with foam scaffolds (VML+Foam group) as compared to animals suffering VML injury without any treatment [Figs. 6(b-ii) and 6(b-iii)]. No signs of severe inflammatory response against the *in vivo* printed scaffolds were observed in the H&E stained samples [Fig. 6(b-iv)]. Further assessments using immunofluorescent techniques revealed areas of regenerated muscle fibers at the intersection of the remnant muscle and scaffold [Fig. 6(b-v)]. Our histological analysis further showed that most of the newly formed myofibers were properly aligned to the remnant fibers. Evaluation of acetylcholine receptors (AchR), a component of neuromuscular junctions, demonstrated a higher number of receptors within the regenerating area following VML treatment with foam scaffolds [Fig. 6(b-vi)]. Staining against CD31 antigen further showed areas of vascularization at the muscle-scaffold interface and within the scaffold [Fig. 6(b-vii)]. Taken together, treatment of an acute VML injury with a foam scaffold promoted composite restoration of the muscle defect, which is improved as compared to soft tissue regeneration offered by less porous scaffolds.[51,52]

To further quantify the functional recovery of the injured muscles, the *in situ* generated forces were measured using a force transducer machine. To evaluate the functional muscle recovery, at 8 weeks post injury, the gastrocnemius muscle was isolated in each mouse and subjected to *in situ* strength testing using a force transducer instrument.[53] The results demonstrated that implantation of a foam scaffold improved both twitch [36.0 ± 7.1 vs 26.8 ± 5.2 mN/mm²; $p = 0.04$; Fig. 6(c)] and tetanic strength [194.4 ± 26.3 vs 155.5 ± 29.7 mN/mm²; $p = 0.03$; Fig. 6(d)] of the gastrocnemius following VML injury as compared to VML injury alone. Muscle forces in VML untreated group were markedly lower than those of Sham group in terms of twitch [42.8 ± 7.7 vs 26.8 ± 5.2 mN/mm²; $p = 0.0004$; Fig. 6(c)] and tetanic strengths [223.8 ± 26.3 vs 155.5 ± 29.7 mN/mm²; $p = 0.0002$; Fig. 6(d)] at 8 weeks post injury, while the differences of these values between Sham and VML+Foam groups were not significant ($p > 0.05$), indicating that *in vivo* printing of foam was enabled the recovery of muscle function to a degree near to that of uninjured muscle.

III. DISCUSSIONS

3D bioprinting technologies have rapidly grown over the last decade. The advancement in bioink development has enabled biomanufacturing of biomimetic tissue-like constructs.[54] Among different
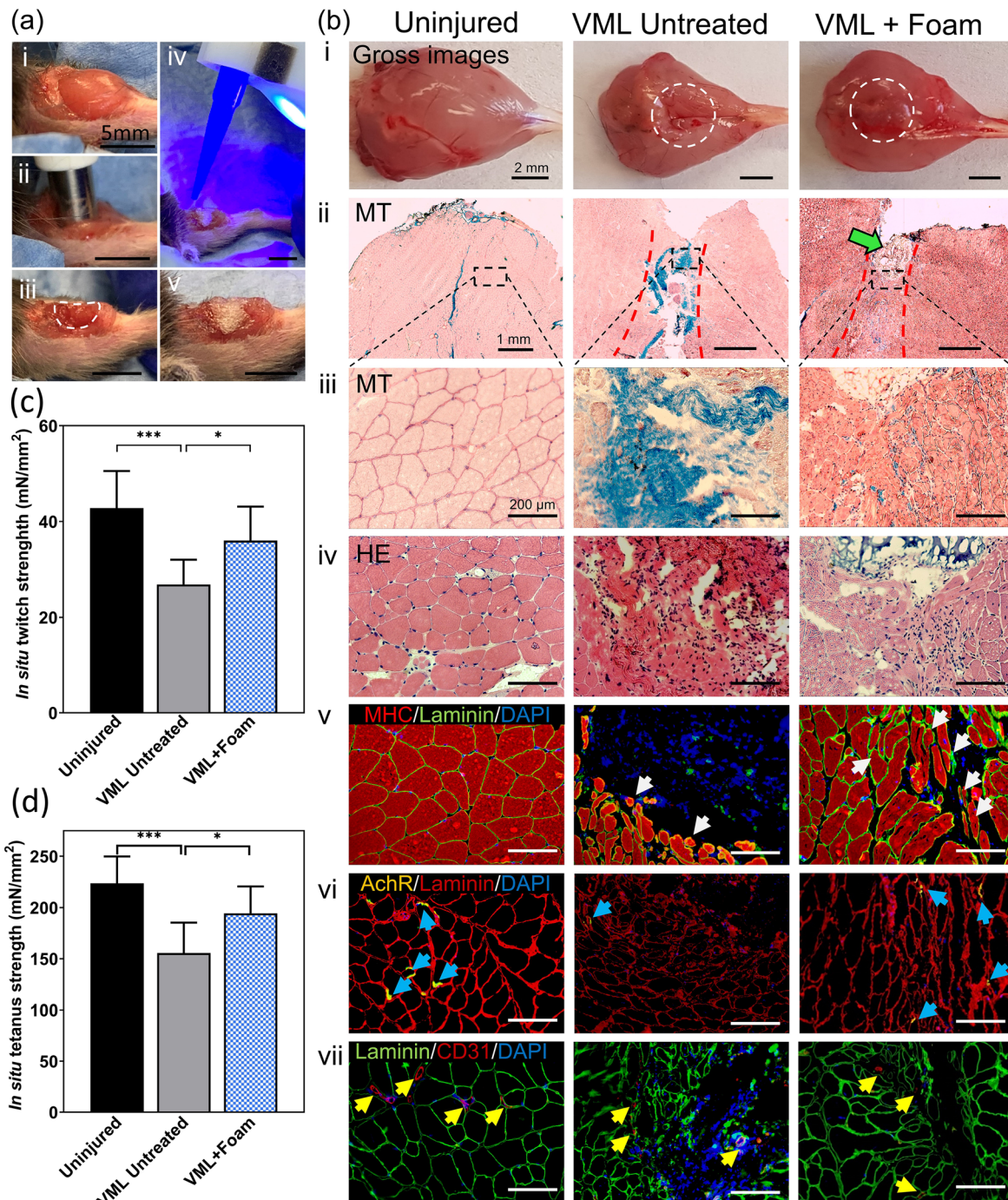
FIG. 6. Functional and histological evaluations of the GelMA foam scaffold bioprinted in a murine model of VML injury. (a) *In vivo* printing into an induced VML wound: (i) uninjured gastrocnemius muscle; (ii) making a full thickness muscle defect using a biopsy punch; (iii) muscle defect after resection to simulate VML injury; (iv) *in vivo* printing of foam bioink; and (v) reconstructed foam scaffold that replicates the geometry of the native muscle. (b) (i) Gross images of the extracted muscles 8 weeks post-surgery, indicating distorted structure of muscle in VML untreated group, and well integration of the foam into the tissue in VML+Foam group. (ii-iv) MT and H&E staining of the samples showing excellent tissue-regeneration at the site of injury (red dashed line) in the group treated by foam vs the fibrosis formation in the untreated group (green arrow shows the remnant foam scaffold). (v) Immunostaining for muscle specific markers (MHC, Laminin) shows well-aligned differentiated regenerating myofibers (white arrows) at the site of injury which are replaced with the scaffold. Along with myogenesis, foam application enabled innervation [(vi), blue arrows], and vascularization [(vii), yellow arrows] at the site of injury as shown by immunostaining for AchR and CD31 markers, respectively. The results of *in situ* isometric twitch (c) and tetanic (d) force measurements of gastrocnemius muscle showing better functional recovery with the application of foam scaffold in skeletal muscle VML injury, compared to the untreated and sham groups.

bioprinting approaches, extrusion 3D bioprinting of hydrogel scaffolds has received significant attention due to its compatibility with a wide range of bioink materials and cell densities.[13] An ideal bioink for 3D bioprinting should offer good printability for the fabrication of 3D constructs with high fidelity, while it needs to provide a favorable environment supporting cellular migration, proliferation, and maturation.

Among various hydrogel-based inks, alginate has been widely used due to its favorable rheological properties and fast cross-linking in the presence of divalent cations.[55,56] However, alginate does not properly support cellular activity due to the lack of cell adhesive moieties and its dense polymeric network.[57,58] Collagen, as the main component of ECM, has a suitable biological efficacy, though its slow cross-linking may limit its application in bioprinting to very simple planar constructs.[59] Therefore, a hydrogel with optimal printability and biocompatibility is an essential requirement for extrusion-based 3D bioprinting.

In recent years, GelMA has attracted increasing attention for tissue engineering applications due to its biocompatibility, bioadhesivity, and ease of photocross-linking.[36,60] However, its low viscosity and relatively slow cross-linking have been a challenge for its applications in extrusion-based 3D bioprinting.[52] Several strategies have been used to improve the printability of GelMA, such as increasing the precursor concentration, partial pre-cross-linking to increase its viscosity, and integration of other hydrogels, such as alginate and gelatin, to improve the rheological properties and facilitate the rapid cross-linking of the hybrid hydrogel.[61,62] However, increasing the precursor concentration may result in reduced cellular activity inside the GelMA scaffold. Partial pre-cross-linking also can make the bioprinting process unreliable, and hybridization may complicate the bioink preparation, printing, and cross-linking, all reduce the printability window.[63,64] Another strategy is the incorporation of nano- or micro-particles to improve the rheological properties of GelMA and make it shear thinning for 3D printing. However, it has been reported that this process can significantly affect the cell ingrowth inside the scaffold.[58] Additionally, limited diffusion of nutrients, oxygen, and waste through the small microporous hydrogel network further diminish the cellular activity inside the conventional GelMA-based scaffolds, specifically when constructs with clinically relevant dimensions are required.[65] It has been reported that the diffusion within hydrogel constructs is very slow and inefficient in millimeter-scale and larger constructs.[66] The small pore size in the GelMA structure further limits the cell infiltration, expansion, and therefore final tissue integration.[65]

To resolve the above-mentioned challenges of GelMA bioprinting, here we introduce multiscale porosity inside the hydrogel precursor to enhance both the printability and cell permissibility of the bioprinted GelMA scaffolds. Inspired by whipped cream production in pastries, we developed porous bioinks through a simple foaming process with high-speed stirring. In this approach, the pore size could be controlled by varying the stirring duration, stirring speed, and concentration of the hydrogel. The GelMA foaming process led to the introduction of spherical bubbles of 50–400 μm size, surrounded by a naturally derived microporous GelMA network. Our results demonstrated that the mechanism of pore formation in the stirring process was shear-induced bubble splitting. In this mechanism, large air bubbles, introduced initially by inserting the tip of the homogenizer inside the solution, were split into smaller bubbles due to the shear stress between the solution layers where the bubbles were located.[67] The

shear stress dominated the surface tension of the bubble and formed smaller independent bubbles consecutively, until the bubbles were smaller than a critical size to be split with shear stress applied to the bubble surface. Increased GelMA concentration and stirring speed directly increased the shear stress, decreasing the bubbles' lower limit size, while increasing the stirring time can offer a more homogeneous pore size dispersion. Overall, our results demonstrated that a 40 s stirring with 22 000 rpm could form an almost homogeneous porous structure in 15% GelMA, with a 75 μm average pore diameter. Since foam instability caused by bubble merging has been a concern in air colloidal systems, PVA, a biocompatible water-soluble polymer, was implemented to enhance the stability of bubbles in the foam and decrease the bubble burst rate during the foam generation process.[68,69] Micrographs from printed filaments of Rhodamine B-loaded GelMA foam containing PVA after their incubating in an aqueous environment demonstrated the formed bubbles during the foaming process, extrusion, and post-cross-linking were stabilized.

The rheological data from foam and hydrogel bioinks showed that the foam experienced much smaller moduli (storage and loss) changes during sol–gel transitions as compared to hydrogel, making its bioprinting parameters more stable and reproducible. Furthermore, the results demonstrated that the viscosity of the foam bioink was much higher than the gel, due to internal friction induced by the presence of packed bubbles, making it much easier to print. The foam bioink was robust and not only could be printed using stationary and fully automated bioprinters, but it also offered rheological properties that one could print and write structures using a handheld device. The ability to print the ink using a handheld printer means that it can be used for direct *in vivo* printing of scaffolds in the defect site. This approach has drawn significant attention recently because it offers a rapid, simple, and controllable treatment procedure while it can overcome the challenges associated with the implantation and fixation of the scaffolds within the defect site through the application of adhesive materials. Our lap shear experiments demonstrated that the foam bioink had a proper adhesion strength ($\sim$6–14 kPa) to the skin tissue and had more flexibility and ductility compared to the hydrogel. This indicates that the foam is a suitable bioink for *in vivo* printing in soft tissue injuries. The foam bioink offered high shape fidelity, structural stability, proper mechanical properties for soft tissue engineering,[43] and strong adhesion to the surrounding tissues *in vitro* and *ex vivo*.

In addition to printability, a bioink needs to support cellular activity and good tissue integration. To evaluate this, we investigated the biocompatibility of the bioinks *in vitro* and *in vivo*. Our *in vitro* results demonstrated that the foam bioink, in contrast to the gel with similar polymeric concentration, supported cellular viability, spreading, and proliferation. These improvements are probably because of the meso- to micro-porous structure within the polymeric networks, which provide enough space for cell expansion and proliferation.[68] The *in vivo* evaluation of foam bioinks 1 week after subcutaneous implantation in rats further indicated a complete implant-tissue integration recognized by a high level of cellular infiltration and neovascularization within the foam scaffold. The rapid foam scaffold remodeling in contrast to the hydrogel can be attributed to the presence of interconnected mesoscale and microscale pores in the scaffold structure. The multiscale interconnected porous structure offers a larger space for the cells to anchor and expand, making the foam a suitable environment for improved cell adhesion, differentiation, and

tissue regeneration. It has been reported that the interconnected structure facilitates cell infiltration and transport of nutrients and waste, and therefore accelerates scaffold-tissue integration and its vascularization and innervation.[70]

A promising application of foam scaffolds may be the treatment of musculoskeletal defects. Substantial VML injuries (usually more than 20% muscle mass loss) results in disrupted tissue architecture and the affected muscle follows a pathologic response resulting in fibrosis,[71] which subsequently leads to poor strength recovery and permanent disability.[72] As a result, a cell-favorable biomaterial with large porosities is required to form a large scaffold at injury site and facilitate the migration of cells from the remnant tissue for regeneration of the tissue to a functional muscle.[52] *In vivo* printing of the foam resulted in significantly improved soft tissue contour following the injury, with restoration of blood vessels, skeletal muscle fibers abutting the area of muscle injury, and neuromuscular junctions. In comparison, although placement of scaffolds without meso-porosities may improve the hypertrophy of remnant muscle fibers and limit fibrosis, they are limited in promoting skeletal muscle regeneration, angiogenesis, or neurogenesis within the scaffold itself.[45,73] This can be attributed to lower capability of cell infiltration inside the scaffolds as a result of lower porosity sizes. Structural improvements detected in histological analysis correlated with improvements in functional recovery of the muscle indicated by muscle strength recovery. Importantly, although foam scaffold placement did not contain preexisting, aligned for nascent tissue to conform to, it allowed for the formation of aligned fibers within the injured area through scaffold remodeling by the cells. This is in agreement with previous studies demonstrating the capability of acellular scaffolds to promote recovery of muscle function post VML injury.[74] The *in vivo* printing of foam scaffolds further offers the additional benefit of being able to conform the scaffold to any shape defect and obviates the need for sutures.

In this study, VML has been used as a defect model for assessment of regeneration potential of pure GelMA foam bioink due to the close proximity of its mechanical properties to native muscle tissues. While results demonstrate promising regeneration and functional recovery of muscle, various growth factors or cells can be incorporated into the foam bioink to boost its regeneration potential. Alternatively, this strategy can be used for regeneration of other tissues, such as skin and bone, by modulating the mechanical properties, incorporating other biomaterials and bioactive reagents, and encapsulated cells. Given the similarity of the foam architecture (as shown in SEM images of Figs. 1 and 2) to bone tissue structure, the addition of osteogenic factors into the foam bioink and adjusting its mechanical properties makes it a promising candidate for bone tissue engineering. While similar structures have been applied in bone tissue engineering, formed through other foaming strategies, such as particulate leaching, particle sintering, and phase separation,[75,76] these strategies are limited in offering a biocompatible printable bioink. Therefore, the proposed strategy in this study can open new avenues in tissue engineering, particularly for musculoskeletal tissues.

Taken together, foam bioinks are rapidly producible, do not require any chemical modifications, robustly incorporate into tissue defects, and can promote their regeneration. As such, foam bioinks are expected to be clinically relevant in regenerative medicine applications.

IV. MATERIALS AND METHODS

Details of the experimental approaches are provided in the supplementary information.

A. Bioink preparation

For preparing foam bioinks, at first, 1% (w/v) PVA was dissolved in DPBS (HyClone) at $100\,°C$; after cooling down to $37\,°C$, 0.3% (w/v) lithium phenyl-2,4,6-trimethylbenzoylphosphinate (LAP) (Sigma) was dissolved in the solution and covered with foil to be protected from light. To prepare different concentrations of GelMA solution, 10%, 15%, and 20% (w/v) of GelMA were dissolved in the solution. GelMA solutions were poured into a 5 ml syringe closed beforehand with a locking tip and were homogenized using a homogenizer (SCILOGEX D160) at different speeds for a specific time. The foam bioink inside the syringes was used for bioprinting. The same GelMA solutions were used to form hydrogel scaffolds as control for all experiments. Printed structures then cross-linked with visible lights using a light-emitting diode (LED) light (395–400 nm, 20 W) for 1 min.

B. Statistical analysis

Displayed data are reported as mean ± standard deviation. GraphPad Prism 8.0 software (San Diego, CA) was used to perform statistical analyses. Column analyses were conducted using two-tailed Student's t-test. Grouped analyses were completed using analyses of variance (ANOVA) testing. Significant ANOVA results underwent Tukey's multiple comparison post-hoc testing. Values of $p < 0.05$ were considered statistically significant. $p < 0.05$ denoted by *, $p < 0.01$ denoted by **, $p < 0.001$ denoted by ***, and a $p < 0.0001$ denoted by ****.

SUPPLEMENTARY MATERIAL

See the supplementary material for additional information on the methods used for material synthesis, physicochemical characterization of the materials, biological assessment of the scaffolds, bioprinting of the developed inks, and the procedures used in the animal studies and the evaluation of the experimental outcomes. Information of the antibodies used in the histological analysis and some data related to the assessment of the mechanical and biological characterization of the scaffolds are also included in the supplementary material.

AUTHOR DECLARATIONS
Conflict of Interest

A.T., M.S., and I.S. declare involvement in InPrint Bio LLC.

Ethics Approval

Muscle injury studies were performed at Brigham and Women's Hospital in accordance with Protocol 2016N000375 and approved by the Institutional Animal Care and Use Committee (IACUC).

Subcutaneous implantation was approved by the IACUC (Protocol No. 2018–076-01C) at the University of California Los Angeles (UCLA).

Author Contributions

A.M., A.T., and N.A. conceived the idea. A.T., N.A, and I.S. designed the experiments. A.M. developed the foaming process, performed physical and mechanical characterization, 3D printing optimization, and *in vitro* cell study. MS Performed the SEM and rheological experiments. M.K. and Y.E. performed the VML animal model study. M.G. synthesized GelMA. A.M. and M.G performed the subcutaneous implantation. I.S., A.T., A.M., N.A., and M.S. helped with the data analysis and interpretation of the results. The manuscript was written by A.M., M.S., and A.T. All authors contributed to the manuscript revision.

DATA AVAILABILITY

All the necessary data that support the findings of this study are available within the article and its supplementary material. Additional data that support the findings of this study are available from the corresponding authors upon reasonable request.

REFERENCES

[1]A. Tamayol, M. Akbari, N. Annabi, A. Paul, A. Khademhosseini, and D. Juncker, "Fiber-based tissue engineering: Progress, challenges, and opportunities," Biotechnol. Adv. **31**(5), 669–687 (2013).

[2]S. M. Naseer, A. Manbachi, M. Samandari, P. Walch, Y. Gao, Y. S. Zhang, F. Davoudi, W. Wang, K. Abrinia, J. M. Cooper, A. Khademhosseini, and S. R. Shin, "Surface acoustic waves induced micropatterning of cells in gelatin methacryloyl (GelMA) hydrogels," Biofabrication **9**(1), 015020 (2017).

[3]T. Abudula, K. Gauthaman, A. Mostafavi, A. Alshahrie, N. Salah, P. Morganti, A. Chianese, A. Tamayol, and A. Memic, "Sustainable drug release from polycaprolactone coated chitin-lignin gel fibrous scaffolds," Sci. Rep. **10**(1), 20428 (2020).

[4]A. Mostafavi, H. Daemi, S. Rajabi, and H. Baharvand, "Highly tough and ultrafast self-healable dual physically crosslinked sulfated alginate-based polyurethane elastomers for vascular tissue engineering," Carbohydr. Polym. **257**, 117632 (2021).

[5]M. Akbari, A. Tamayol, S. Bagherifard, L. Serex, P. Mostafalu, N. Faramarzi, M. H. Mohammadi, and A. Khademhosseini, "Textile technologies and tissue engineering: A path toward organ weaving," Adv. Healthcare Mater. **5**(7), 751–766 (2016).

[6]A. Nasajpour, A. Mostafavi, A. Chlanda, C. Rinoldi, S. Sharifi, M. S. Ji, M. Ye, S. J. Jonas, W. Swieszkowski, and P. S. Weiss, "Cholesteryl ester liquid crystal nanofibers for tissue engineering applications," ACS Mater. Lett. **2**(9), 1067–1073 (2020).

[7]H.-W. Kang, S. J. Lee, I. K. Ko, C. Kengla, J. J. Yoo, and A. Atala, "A 3D bioprinting system to produce human-scale tissue constructs with structural integrity," Nat. Biotechnol. **34**(3), 312–319 (2016).

[8]A. Farzin, A. K. Miri, F. Sharifi, N. Faramarzi, A. Jaberi, A. Mostafavi, R. Solorzano, Y. S. Zhang, N. Annabi, A. Khademhosseini, and A. Tamayol, "3D-printed sugar-based stents facilitating vascular anastomosis," Adv. Healthcare Mater. **7**(24), e1800702 (2018).

[9]S. V. Murphy and A. Atala, "3D bioprinting of tissues and organs," Nat. Biotechnol. **32**(8), 773–785 (2014).

[10]C. Chávez-Madero, M. D. de León-Derby, M. Samandari, C. F. Ceballos-González, E. J. Bolívar-Monsalve, C. Mendoza-Buenrostro, S. Holmberg, N. A. Garza-Flores, M. A. Almajhadi, I. González-Gamboa, J. F. Yee-de León, S. O. Martínez-Chapa, C. A. Rodríguez, H. K. Wickramasinghe, M. Madou, D. Dean, A. Khademhosseini, Y. S. Zhang, M. M. Alvarez, and G. Trujillo-de Santiago, "Using chaotic advection for facile high-throughput fabrication of ordered multilayer micro- and nanostructures: Continuous chaotic printing," Biofabrication **12**(3), 035023 (2020).

[11]M. Samandari, F. Alipanah, K. Majidzadeh-A, M. M. Alvarez, G. Trujillo-de Santiago, and A. Tamayol, "Controlling cellular organization in bioprinting through designed 3D microcompartmentalization," Appl. Phys. Rev. **8**(2), 021404 (2021).

[12]S. Gerdes, A. Mostafavi, S. Ramesh, A. Memic, I. V. Rivero, P. Rao, and A. Tamayol, "Process-structure-quality relationships of three-dimensional printed poly(caprolactone)-hydroxyapatite scaffolds," Tissue Eng. Part A **26**(5–6), 279–291 (2020).

[13]G.-L. Ying, N. Jiang, S. Maharjan, Y.-X. Yin, R.-R. Chai, X. Cao, J.-Z. Yang, A. K. Miri, S. Hassan, and Y. S. Zhang, "Aqueous two-phase emulsion bioink-enabled 3D bioprinting of porous hydrogels," Adv. Mater. **30**(50), e1805460 (2018).

[14]A. Mostafavi, J. Quint, C. Russell, and A. Tamayol, "Nanocomposite hydrogels for tissue engineering applications," in *Biomaterials for Organ and Tissue Regeneration* (Elsevier, 2020), pp. 499–528.

[15]M. Sun, X. Sun, Z. Wang, S. Guo, G. Yu, and H. Yang, "Synthesis and properties of gelatin methacryloyl (GelMA) hydrogels and their recent applications in load-bearing tissue," Polymers **10**(11), 1290 (2018).

[16]A. K. Miri, H. G. Hosseinabadi, B. Cecen, S. Hassan, and Y. S. Zhang, "Permeability mapping of gelatin methacryloyl hydrogels," Acta Biomater **77**, 38–47 (2018).

[17]N. Annabi, A. Tamayol, J. A. Uquillas, M. Akbari, L. E. Bertassoni, C. Cha, G. Camci-Unal, M. R. Dokmeci, N. A. Peppas, and A. Khademhosseini, "25th anniversary article: Rational design and applications of hydrogels in regenerative medicine," Adv. Mater. **26**(1), 85–123 (2014).

[18]K. Elkhoury, C. S. Russell, L. Sanchez-Gonzalez, A. Mostafavi, T. J. Williams, C. Kahn, N. A. Peppas, E. Arab-Tehrany, and A. Tamayol, "Soft-nanoparticle functionalization of natural hydrogels for tissue engineering applications," Adv. Healthcare Mater. **8**(18), e1900506 (2019).

[19]O. Lieleg and K. Ribbeck, "Biological hydrogels as selective diffusion barriers," Trends Cell Biol. **21**(9), 543–551 (2011).

[20]C. S. Verbeke and D. J. Mooney, "Injectable, pore-forming hydrogels for in vivo enrichment of immature dendritic cells," Adv. Healthcare Mater. **4**(17), 2677–2687 (2015).

[21]V. Keskar, N. W. Marion, J. J. Mao, and R. A. Gemeinhart, "In vitro evaluation of macroporous hydrogels to facilitate stem cell infiltration, growth, and mineralization," Tissue Eng. Part A **15**(7), 1695–1707 (2009).

[22]J. Zeltinger, J. K. Sherwood, D. A. Graham, R. Müeller, and L. G. Griffith, "Effect of pore size and void fraction on cellular adhesion, proliferation, and matrix deposition," Tissue Eng. **7**(5), 557–572 (2001).

[23]Y. He, F. Yang, H. Zhao, Q. Gao, B. Xia, and J. Fu, "Research on the printability of hydrogels in 3D bioprinting," Sci. Rep. **6**(1), 29977 (2016).

[24]M. M. Nava, L. Draghi, C. Giordano, and R. Pietrabissa, "The effect of scaffold pore size in cartilage tissue engineering," J. Appl. Biomater. Funct. Mater. **14**(3), e223–e229 (2016).

[25]L. G. Griffith, "Tissue engineering–current challenges and expanding opportunities," Science **295**(5557), 1009–1014 (2002).

[26]W. Zhu, X. Qu, J. Zhu, X. Ma, S. Patel, J. Liu, P. Wang, C. S. E. Lai, M. Gou, and Y. Xu, "Direct 3D bioprinting of prevascularized tissue constructs with complex microarchitecture," Biomaterials **124**, 106–115 (2017).

[27]N. Huebsch, E. Lippens, K. Lee, M. Mehta, S. T. Koshy, M. C. Darnell, R. M. Desai, C. M. Madl, M. Xu, X. Zhao, O. Chaudhuri, C. Verbeke, W. S. Kim, K. Alim, A. Mammoto, D. E. Ingber, G. N. Duda, and D. J. Mooney, "Matrix elasticity of void-forming hydrogels controls transplanted-stem-cell-mediated bone formation," Nat. Mater. **14**(12), 1269–1277 (2015).

[28]A. Autissier, C. Le Visage, C. Pouzet, F. Chaubet, and D. Letourneur, "Fabrication of porous polysaccharide-based scaffolds using a combined freeze-drying/cross-linking process," Acta Biomater. **6**(9), 3640–3648 (2010).

[29]C. Ji, N. Annabi, A. Khademhosseini, and F. Dehghani, "Fabrication of porous chitosan scaffolds for soft tissue engineering using dense gas CO2," Acta Biomater. **7**(4), 1653–1664 (2011).

[30]S. B. Lee, Y. H. Kim, M. S. Chong, S. H. Hong, and Y. M. Lee, "Study of gelatin-containing artificial skin V: Fabrication of gelatin scaffolds using a salt-leaching method," Biomaterials **26**(14), 1961–1968 (2005).

[31]S. Van Vlierberghe, G. J. Graulus, S. Keshari Samal, I. Van Nieuwenhove, and P. Dubruel, "Porous hydrogel biomedical foam scaffolds for tissue repair," in

Biomedical Foams for Tissue Engineering Applications (Woodhead Publishing, 2014), pp. 335–390.

[32]P. Netti, *Biomedical Foams for Tissue Engineering Applications* (Elsevier, 2014), p. 446.

[33]L. Shao, Q. Gao, C. Xie, J. Fu, M. Xiang, Z. Liu, L. Xiang, and Y. He, "Sacrificial microgel-laden bioink-enabled 3D bioprinting of mesoscale pore networks," Bio-Des. Manuf. **3**(1), 30–39 (2020).

[34]A. Hori, Y. Watabe, M. Yamada, Y. Yajima, R. Utoh, and M. Seki, "One-step formation of microporous hydrogel sponges encapsulating living cells by utilizing bicontinuous dispersion of aqueous polymer solutions," ACS Appl. Bio Mater. **2**(5), 2237–2245 (2019).

[35]T. Salvador, M. B. Oliveira, and J. F. Mano, "Leachable-free fabrication of hydrogel foams enabling homogeneous viability of encapsulated cells in large-volume constructs," Adv. Healthcare Mater. **9**(20), e2000543 (2020).

[36]K. Yue, G. Trujillo-de Santiago, M. M. Alvarez, A. Tamayol, N. Annabi, and A. Khademhosseini, "Synthesis, properties, and biomedical applications of gelatin methacryloyl (GelMA) hydrogels," Biomaterials **73**, 254–271 (2015).

[37]A. Assmann, A. Vegh, M. Ghasemi-Rad, S. Bagherifard, G. Cheng, E. S. Sani, G. U. Ruiz-Esparza, I. Noshadi, A. D. Lassaletta, and S. Gangadharan, "A highly adhesive and naturally derived sealant," Biomaterials **140**, 115–127 (2017).

[38]N. Annabi, D. Rana, E. S. Sani, R. Portillo-Lara, J. L. Gifford, M. M. Fares, S. M. Mithieux, and A. S. Weiss, "Engineering a sprayable and elastic hydrogel adhesive with antimicrobial properties for wound healing," Biomaterials **139**, 229–243 (2017).

[39]B. Saleh, H. K. Dhaliwal, R. Portillo-Lara, E. Shirzaei Sani, R. Abdi, M. M. Amiji, and N. Annabi, "Local immunomodulation using an adhesive hydrogel loaded with miRNA-laden nanoparticles promotes wound healing," Small **15**(36), 1902232 (2019).

[40]C. S. Russell, A. Mostafavi, J. P. Quint, A. C. Panayi, K. Baldino, T. J. Williams, J. G. Daubendiek, V. H. Sánchez, Z. Bonick, M. Trujillo-Miranda, S. R. Shin, O. Pourquie, S. Salehi, I. Sinha, and A. Tamayol, "In situ printing of adhesive hydrogel scaffolds for the treatment of skeletal muscle injuries," ACS Appl. Bio Mater. **3**(3), 1568–1579 (2020).

[41]E. Mendizabal, J. R. Castellanos-Ortega, and J. E. Puig, "A method for selecting a polyvinyl alcohol as stabilizer in suspension polymerization," Colloids Surf. **63**(3–4), 209–217 (1992).

[42]P. A. Tran, H. T. Nguyen, K. Fox, and N. Tran, "In vitro cytotoxicity of iron oxide nanoparticles: Effects of chitosan and polyvinyl alcohol as stabilizing agents," Mater. Res. Express **5**(3), 035051 (2018).

[43]X. Zhai and W. Chen, "Compressive mechanical response of porcine muscle at intermediate (10 0/s-10 2/s) strain rates," Exp. Mech. **59**(9), 1299–1305 (2019).

[44]G. Ying, N. Jiang, C. Yu, and Y. S. Zhang, "Three-dimensional bioprinting of gelatin methacryloyl (GelMA)," Bio-Des. Manuf. **1**(4), 215–224 (2018).

[45]J. P. Quint, A. Mostafavi, Y. Endo, A. Panayi, C. S. Russell, A. Nourmahnad, C. Wiseman, L. Abbasi, M. Samandari, A. Sheikhi, K. Nuutila, I. Sinha, and A. Tamayol, "In vivo printing of nanoenabled scaffolds for the treatment of skeletal muscle injuries," Adv. Healthcare Mater. **10**(10), 2002152 (2021).

[46]K. Nuutila, M. Samandari, Y. Endo, Y. Zhang, J. Quint, T. A. Schmidt, A. Tamayol, and I. Sinha, "In vivo printing of growth factor-eluting adhesive scaffolds improves wound healing," Bioact. Mater. (to be published), available at https://www.sciencedirect.com/science/article/pii/S2452199X21003169.

[47]C. Li, L. Ouyang, J. P. Armstrong, and M. M. Stevens, "Advances in the fabrication of biomaterials for gradient tissue engineering," Trends Biotechnol. **39**(2), 150–164 (2021).

[48]E. Shirzaei Sani, A. Kheirkhah, D. Rana, Z. Sun, W. Foulsham, A. Sheikhi, A. Khademhosseini, R. Dana, and N. Annabi, "Sutureless repair of corneal injuries using naturally derived bioadhesive hydrogels," Sci. Adv. **5**(3), eaav1281 (2019).

[49]W. M. Southern, A. S. Nichenko, K. F. Tehrani, M. J. McGranahan, L. Krishnan, A. E. Qualls, N. T. Jenkins, L. J. Mortensen, H. Yin, and A. Yin, "PGC-1α overexpression partially rescues impaired oxidative and contractile pathophysiology following volumetric muscle loss injury," Sci. Rep. **9**(1), 4079 (2019).

[50]S. M. Greising, G. L. Warren, W. M. Southern, A. S. Nichenko, A. E. Qualls, B. T. Corona, and J. A. Call, "Early rehabilitation for volumetric muscle loss injury augments endogenous regenerative aspects of muscle strength and oxidative capacity," BMC Musculoskeletal Disord. **19**(1), 173 (2018).

[51]S. M. Greising, J. C. Rivera, S. M. Goldman, A. Watts, C. A. Aguilar, and B. T. Corona, "Unwavering pathobiology of volumetric muscle loss injury," Sci. Rep. **7**(1), 13179 (2017).

[52]M. Samandari, J. Quint, A. Rodríguez-delaRosa, I. Sinha, O. Pourquié, and A. Tamayol, "Bioinks and bioprinting strategies for skeletal muscle tissue engineering," Adv. Mater. (to be published).

[53]K. W. VanDusen, B. C. Syverud, M. L. Williams, J. D. Lee, and L. M. Larkin, "engineered skeletal muscle units for repair of volumetric muscle loss in the tibialis anterior muscle of a rat," Tissue Eng. Part A **20**(21–22), 2920–2930 (2014).

[54]M. A. Heinrich, W. Liu, A. Jimenez, J. Yang, A. Akpek, X. Liu, Q. Pi, X. Mu, N. Hu, R. M. Schiffelers, J. Prakash, J. Xie, and Y. S. Zhang, "3D bioprinting: From benches to translational applications," Small **15**(23), e1805510 (2019).

[55]M. Samandari, F. Alipanah, S. H. Javanmard, and A. Sanati-Nezhad, "One-step wettability patterning of PDMS microchannels for generation of monodisperse alginate microbeads by in Situ external gelation in double emulsion microdroplets," Sens. Actuators B: Chem. **291**, 418–425 (2019).

[56]M. Samandari, F. Alipanah, A. Tamayol, S. H. Javanmard, and A. Sanati-Nezhad, "Controlled self-assembly of microgels in microdroplets," Sens. Actuators B: Chem. **348**, 130693 (2021).

[57]K. Markstedt, A. Mantas, I. Tournier, H. Martínez Ávila, D. Hägg, and P. Gatenholm, "3D bioprinting human chondrocytes with nanocellulose-alginate bioink for cartilage tissue engineering applications," Biomacromolecules **16**(5), 1489–1496 (2015).

[58]Q. Gao, X. Niu, L. Shao, L. Zhou, Z. Lin, A. Sun, J. Fu, Z. Chen, J. Hu, Y. Liu, and Y. He, "3D printing of complex GelMA-based scaffolds with nanoclay," Biofabrication **11**(3), 035006 (2019).

[59]A. Lee, A. R. Hudson, D. J. Shiwarski, J. W. Tashman, T. J. Hinton, S. Yerneni, J. M. Bliley, P. G. Campbell, and A. W. Feinberg, "3D bioprinting of collagen to rebuild components of the human heart," Science **365**(6452), 482–487 (2019).

[60]L. Shao, Q. Gao, H. Zhao, C. Xie, J. Fu, Z. Liu, M. Xiang, and Y. He, "Fiber-based mini tissue with morphology-controllable GelMA microfibers," Small **14**(44), e1802187 (2018).

[61]D. B. Kolesky, R. L. Truby, A. S. Gladman, T. A. Busbee, K. A. Homan, and J. A. Lewis, "3D bioprinting of vascularized, heterogeneous cell-laden tissue constructs," Adv. Mater. **26**(19), 3124–3130 (2014).

[62]A. Tamayol, A. H. Najafabadi, B. Aliakbarian, E. Arab-Tehrany, M. Akbari, N. Annabi, D. Juncker, and A. Khademhosseini, "Hydrogel templates for rapid manufacturing of bioactive fibers and 3D constructs," Adv. Healthcare Mater. **4**(14), 2146–2153 (2015).

[63]C. Colosi, S. R. Shin, V. Manoharan, S. Massa, M. Costantini, A. Barbetta, M. R. Dokmeci, M. Dentini, and A. Khademhosseini, "Microfluidic bioprinting of heterogeneous 3D tissue constructs using low-viscosity bioink," Adv. Mater. **28**(4), 677–684 (2016).

[64]J. Yin, M. Yan, Y. Wang, J. Fu, and H. Suo, "3D bioprinting of low-concentration cell-laden gelatin methacrylate (GelMA) bioinks with a two-step cross-linking strategy," ACS Appl. Mater. Interfaces **10**(8), 6849–6857 (2018).

[65]D. R. Griffin, W. M. Weaver, P. O. Scumpia, D. Di Carlo, and T. Segura, "Accelerated wound healing by injectable microporous gel scaffolds assembled from annealed building blocks," Nat. Mater. **14**(7), 737–744 (2015).

[66]D. Gholobova, L. Terrie, M. Gerard, H. Declercq, and L. Thorrez, "Vascularization of tissue-engineered skeletal muscle constructs," Biomaterials **235**, 119708 (2020).

[67]W. Li, H. Guo, Q. Huang, P. Han, Y. Hou, and W. Zou, "Effect of stirring rate on microstructure and properties of microporous mullite ceramics," J. Mater. Process. Technol. **261**, 159–163 (2018).

[68]G. Ying, N. Jiang, C. Parra-Cantu, G. Tang, J. Zhang, H. Wang, S. Chen, N. P. Huang, J. Xie, and Y. S. Zhang, "Bioprinted injectable hierarchically porous gelatin methacryloyl hydrogel constructs with shape-memory properties," Adv. Funct. Mater. **30**(46), 2003740 (2020).

[69]B. Dehdari, R. Parsaei, M. Riazi, N. Rezaei, and S. Zendehboudi, "New insight into foam stability enhancement mechanism, using polyvinyl alcohol (PVA) and nanoparticles," J. Mol. Liq. **307**, 112755 (2020).

[70]J. R. Woodard, A. J. Hilldore, S. K. Lan, C. J. Park, A. W. Morgan, J. A. C. Eurell, S. G. Clark, M. B. Wheeler, R. D. Jamison, and A. J. Wagoner Johnson, "The mechanical properties and osteoconductivity of hydroxyapatite bone scaffolds with multi-scale porosity," Biomaterials **28**(1), 45–54 (2007).

[71]S. E. Anderson, W. M. Han, V. Srinivasa, M. Mohiuddin, M. A. Ruehle, J. Y. Moon, E. Shin, C. L. San Emeterio, M. E. Ogle, and E. A. Botchwey,

"Determination of a critical size threshold for volumetric muscle loss in the mouse quadriceps," Tissue Eng. Part C: Methods **25**(2), 59–70 (2019).

[72]B. T. Corona, J. C. Rivera, J. G. Owens, J. C. Wenke, and C. R. Rathbone, "Volumetric muscle loss leads to permanent disability following extremity trauma," J. Rehabil. Res. Develop. **52**(7), 785–792 (2015).

[73]A. C. Panayi, L. Smit, N. Hays, K. Udeh, Y. Endo, B. Li, D. Sakthivel, A. Tamayol, R. L. Neppl, and D. P. Orgill, "A porous collagen-GAG scaffold promotes muscle regeneration following volumetric muscle loss injury," Wound Repair Regener. **28**(1), 61–74 (2020).

[74]B. M. Sicari, J. P. Rubin, C. L. Dearth, M. T. Wolf, F. Ambrosio, M. Boninger, N. J. Turner, D. J. Weber, T. W. Simpson, and A. Wyse, "An acellular biologic scaffold promotes skeletal muscle formation in mice and humans with volumetric muscle loss," Sci. Transl. Med. **6**(234), 234ra58 (2014).

[75]G. L. Koons, M. Diba, and A. G. Mikos, "Materials design for bone-tissue engineering," Nat. Rev. Mater. **5**(8), 584–603 (2020).

[76]M. N. Collins, G. Ren, K. Young, S. Pina, R. L. Reis, and J. M. Oliveira, "Scaffold fabrication technologies and structure/function properties in bone tissue engineering," Adv. Funct. Mater. **31**(21), 2010609 (2021).